A Method for the Analysis of the Nano- and Micromorphology of Printed Structures on Flexible Polymer Films

Analysis of the cross section of inkjet-printed conductive traces on PET film substrates based on ultramicrotome sectioning and SEM imaging.

Martin Ungerer[1], Waldemar Spomer[1], Irene Wacker[2], Rasmus Schröder[2,3], Ulrich Gengenbach[1]

[1] Institute for Applied Computer Science (IAI), Karlsruhe Institute of Technology (KIT),
Eggenstein-Leopoldshafen, Germany
[2] Centre for Advanced Materials (CAM), University Heidelberg, Heidelberg, Germany
[3] CellNetworks, BioQuant, University Hospital Heidelberg, Heidelberg, Germany
e-mail: ungerer@kit.edu

Abstract—**The development of smart sensor systems, wearables or internet of things devices necessitates new fabrication technologies. The challenge is to meet requirements such as low-cost, flexibility, reproducibility and capability for large area fabrication. Fabricating conductive microstructures on polymer films by additive processes like inkjet printing has become increasingly important for these applications in the last decade. Additive processes are potentially more ecofriendly than conventional electronics fabrication processes but printing has still not reached wider implementation in industry. One of the potential reasons is the still insufficient reliability of printed components that must sustain electrical, thermal, mechanical and chemical stress. This reliability of printed products is influenced by a vast number of factors and process parameters. The impact of a certain parameter on the product's reliability can so far not be defined precisely. Besides functional testing, the examination of cross sections of printed structures can lead to a more detailed understanding of their morphology and may entail information for the optimization of the fabrication process. Regarding the requirements, the nano- and microstructure of printed structures has to be analyzed. In the present work, a method is described for the investigation of nano- and microstructures of inkjet-printed conductive traces on polymer substrates by means of scanning electron microscopy of cross sections prepared by ultramicrotome sectioning.**

Keywords-Inkjet-printing; silver nanoparticle ink; polyethylene terephthalate; sintering; ultramicrotome sectioning; imaging by scanning electron microscopy; cross section of conductive traces; microstructure; nanoparticle density.

I. INTRODUCTION

Currently, printing of electronically functional components represents an important field of study in regard of which not only fabrication processes have to be investigated but also methods for the analysis of the reliability of printed devices [1]. In the last decade, printing technologies have become more and more important in research and development for flexible electronics [2]. The objective is to replace conventional subtractive fabrication processes of printed circuit board (PCB) manufacturing by additive processes. Printing processes can be used to fabricate conductive structures, as well as more complex electronic components on flexible polymer films.

The analysis of inkjet-printed conductive structures on polymer substrates in terms of morphology and nanostructure is essential for the assessment of reliability and reproducibility in printed electronics [1]. Established preparation methods for nanostructure analysis are Focused Ion Beam (FIB) milling and ultramicrotome sectioning.

A. Preparation methods for analyzing cross sections of printed structures on polymer films

In FIB milling the material is being etched by a beam of focused Gallium ions, with removal rates of a few µm³/minute and a depth resolution in the range of 5 nanometres [3]. Usually, the FIB instrument is combined with a scanning electron microscope (SEM), so that the new by FIB etching prepared sample surface can be immediately imaged (FIBSEM). Repeated FIB etching and imaging allows inspection of sample volumes, but still on a very limited scale. Moreover the impact of the Gallium ions may, depending on the sample material, create severe damage on and below the milled surface [3]. This includes local amorphization, heating damage and Ga implantation. Chain scission, cross-linking and chain shrinkage have been observed, effects which may transform the structure and crystallinity of polymers [4]. Another aspect is that repeating etching and imaging steps in a FIBSEM the prepared sample surface is continuously being destroyed with the next etching step, hence lost for other imaging modalities.

Ultramicrotome sectioning means embedding the sample in a polymer and cutting thin slices, called sections, with a diamond knife. Section width is limited by the width of the diamond knife, which may reach up to several millimetres. Thus, ultramicrotome sectioning is applicable for structural elucidation of larger volumes than FIB milling. Its depth resolution is however limited by the minimum section thickness achievable for the given combination of sample and embedding material, typically 30 to 200 nm. After

cutting the sections float on the water surface of the knife boat behind the diamond knife edge from where they can be picked up and transferred onto the substrate (glass cover slip, silicon wafer, TEM-grid). Depending on the substrate the sections are then available for different imaging modalities such as light microscopy, SEM or transmission electron microscopy (TEM). Proper embedding of the sample is a challenge; the embedding material stiffness should be compatible with the stiffness of the sample. Distortion of the nanostructure of the sample, e.g., swelling of porous materials due to embedding has to be avoided [4]. Loosely connected particles in the sample may be detached and smeared across the section during cutting. Moreover, mechanical stresses during cutting may lead to deformations and structural alterations.

Melo compares FIB milling and ultramicrotome sectioning for sample preparation for analytical microscopy of the cathode layer of a polymer electrolyte fuel cell and shows the drawbacks of FIB milling and the challenges for ultramicrotome sectioning [4].

The requirements for sample preparation for the structural elucidation of printed electronic structures fabricated in our lab are

- potential for larger sample volumes (a few hundred microns up to a few millimetres width/depth and up to a hundred microns thickness)
- analysis of the samples with different imaging modalities (light microscopy and electron microscopy)

Hence, ultramicrotome sectioning has been selected as method for sample preparation for analysis of printed traces.

B. Functional printing vs. conventional PCB fabrication

A number of printing technologies were transferred from the realm of graphic printing to electronics manufacturing in the last decade. Manufacturing processes can be categorized into processes for mass production and processes for single part or small series production. In the same way, printing processes can be also classified with regard to process productivity. Conventional printing processes based on printing tools (stencils, print cylinders) are well suited for large-scale production whereas, tool-less, non-impact printing processes are more suited to individual part up to small series manufacturing and research applications [5] [6].

Conventional, subtractive PCB fabrication requires a complex process sequence with electroplating, lithography and etching steps based on a fair amount of toxic chemicals. Printing processes usually need one single additive fabrication step followed by an additional curing process in order to create conductive traces on a substrate [7] [8]. Thus, material usage is optimized and the toxic waste accumulated in subtractive processing is eliminated [9]. Printing allows faster, cleaner, cheaper and more environmentally friendly fabrication of PCB's than conventional processes [8]. Additionally, printing enables large area processing of flexible polymer substrates at low temperatures and ambient conditions [10].

The implementation of printing processes for a desired electronic function in microstructure resolution demands careful selection of the three main process components - ink, substrate and printing system. These components have to be precisely tuned to get optimum conditions for realizing features with high reproducibility [5].

C. Ink materials

There exists a number of ink materials to realize electronic functions like resistors, capacitors [11] or transistors [12]. A fundamental element in printed electronics however are conductive traces [7]. They have to provide high conductivities in order to minimize power loss. Currently, there are two main ink types for printing conductive traces available. One type are metal organic decomposition (MOD) inks, with oxidized metal ions as main component [13]. The most prevalent type are nanoparticle inks, where the particles are dispersed in solvents and stabilized by an organic capping agent against agglomeration [14].

Due to their high conductivity, silver-based inks are most widely used [9]. For printed silver nanoparticle traces a conductivity of about 10 % of bulk silver is applicable for many applications [15].

Typically, the particle size of such inks can be found in the range of 10 to 80 nm. Small nanoparticle sizes are desirable, as the nanoparticle size severely influences the curing process, due to melting point depression; the smaller the particles, the lower the melting point compared to the bulk material [16] [17].

D. Printing substrate materials

For printed flexible electronic applications low cost polyethylene terephthalate (PET) substrates are widely used. The base materials have a glass-transition temperature (T_g) of 78 °C and a melting point of 255 °C [18] [19]. Commercially available PET films, e.g., Melinex® ST from DuPont Teijin Films are often used in printed electronic applications. Such PET substrates are thermoplastic semi-crystalline polymer films whose maximum working temperature for printing and sintering processes (T_{max}) of about 150 °C is largely independent of their T_g due to a heat-stabilization [18] [19] [20]. Semi-crystalline polymer films have better resistances against solvents than amorphous polymers [20].

E. Inkjet-printing

Drop-on-demand (DoD) piezo inkjet printing is the most widespread non-impact printing principle in the field of printed electronics [10]. It allows direct, mask-less and vectorial printing of layouts on flexible polymer films [5]. The layouts are created by computer-aided design (CAD) tools. With regard to printability the interaction between print head and ink is of crucial importance. Relevant ink parameters are viscosity, surface energy, density, particle size and particle stability [7] [8]. In order to prevent print head nozzle clogging a particle diameter of less than 1 % of the nozzle diameter is recommended [21].

Inkjet-printing often produces non-uniform, low edge quality and non-reproducible morphology compared to conventional electronics fabrication processes [22] [23]. In order to obtain an optimum line quality, the important printing parameters that need to be controlled are the droplet velocity (v_d), the frequency of droplet generation (f_d), the distance between two adjacent droplets (d_d) on the substrate, the substrate temperature (T_s) and substrate surface properties [24] [25].

F. Curing of printed structures

After the printing process, the resulting structures must be cured in order to get the desired electrical conductivity [15]. First, the ink solvent has to be evaporated; then, the organic stabilizing shell has to be removed. During sintering, a percolation-based network of conductive paths is established due to sporadic agglomeration of particles [15]. At higher temperatures, sintering necks improve the conductivity, the coalescence of the particles leads to a higher metal density of the printed feature [26]. High conductivities have been achieved by means of an oven sintering regime with 30 minutes or more at temperatures above 250 °C [2].

Despite the lower melting point of nanoparticles compared to the bulk material, a sintering regime required for such an increased conductivity is not compatible with many of the widely used low-cost polymer substrates, e.g., PET [27].

Therefore, low temperature sintering methods are taken into consideration that allow either sintering at room temperature (commonly known as chemical sintering) or selective sintering where only the printed structure that needs to be cured is heated while the substrate stays at moderate temperatures [2]. Selective sintering methods are photonic flash sintering, laser sintering, plasma sintering, microwave sintering and electrical current sintering [2] [15].

Chemical sintering comprises, among other methods, sintering triggered by additives in the ink, embedded in the substrate material or coated on its surface [28].

G. Properties of printed structures

In view of the manifold applications of printed structures, such as conductors and passive components, not only their electrical characteristics must be considered, but also their mechanical and chemical properties. Printed conductive traces have to withstand mechanical, chemical und thermal stresses that can influence their inherent porous nanostructure and thereby impair the reliability. Particularly, adhesion to the substrate, bendability and fatigue resistance are important properties of printed structures for applications on flexible polymer substrates. Sintering conditions substantially influence mechanical properties, such as fatigue resistance [29].

H. Hybrid electronics

To date, many electronic functional elements besides conductive traces such as resistors, capacitors, transistors, organic light emitting diodes (OLED), organic photovoltaics (OPV) and sensors have been realized by printing technologies. However, it is currently not possible to achieve the performance of silicon electronic devices; e.g., the switching frequencies of printed transistors are still several orders of magnitude lower than their silicon counterparts.

Moreover, highly integrated circuits such as microcontrollers cannot yet be realized by printing. Therefore, a hybrid approach for the fabrication of more complex electronic systems on flexible polymer substrates seems to be an interesting solution in the medium term to overcome the still low performance of printed complex elements [30] [31]. Marjanović et al. define hybrid electronic integration as the combination of printed components and surface-mount technology (SMT) devices on foils [30].

For demonstration of a hybrid intralayer-integration approach, the conductive trace structure of a flip-flop circuit shown in [31] was first printed with silver nanoparticle ink on a PET film.

Then SMT components were connected to the conductive traces with silver flake based conductive adhesive. Figure 1 shows the realized flip-flop circuit. Tests with these circuits indicated that the system is sensitive to mechanical stress such as bending. Either the conductive adhesive that connects the SMT components fails or the conductive traces crack or delaminate from the substrate. In order to improve the structure's resistance to mechanical stress, the microstructure of the printed traces has to be investigated, as it directly affects the mechanical properties of the printed feature and is of high importance for reliable circuits [32].

After this introduction to hybrid electronics based on functional printing, in Section II, the materials and methods are described that were used for realizing test structures. In Section II.A, the analysis method is outlined, in Section II.B, the test structure is described, in Section II.C, the applied inkjet printer, the silver ink and the PET substrate are presented. Section II.D illustrates the printing process and Section II.E the sample preparation that is needed for the analysis of the cross sections. In Section III, the results of the printing process (Section III.A), the sample preparation (Section III.B) and the SEM analysis of the fabricated cross sections (Section III.C) are outlined. Finally, Section IV gives a conclusion and an outlook.
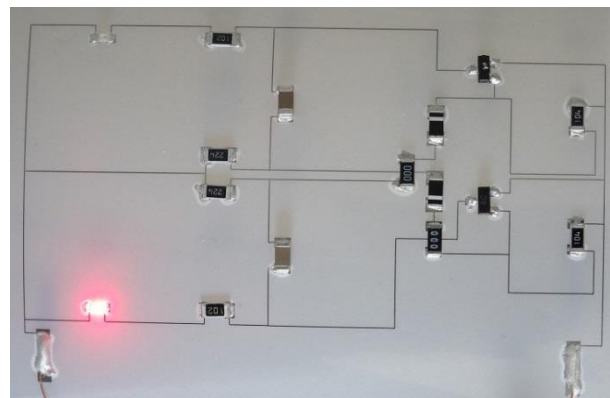

Figure 1. Flip-flop circuit with printed conductive traces and mounted SMT-components

II. MATERIALS AND METHODS

A. Analysis workflow

The method for the analysis of the nano- and microstructure of printed structures on flexible polymer films demonstrated in the present paper is based on a workflow composed of the process steps for sample preparation, the ultrathin sectioning and the analysis itself. Figure 2 shows the workflow of this method. After printing and curing of a test structure on a flexible polymer substrate, rectangular samples were taken. These samples were embedded into an epoxy resin and cured subsequently. Afterwards, the resulting sample blocks were trimmed and sectioned with the ultramicrotome. Scanning electron microscopy (SEM) images were taken from the sections and analyzed afterwards.

B. Test structure

A test structure was defined for the electrical and mechanical evaluation of the properties of different ink-substrate-printer-combinations and different processing parameters. The test structure conceived for electrical and mechanical characterization consists of a 45 mm long conductive trace (L) that connects two contact pads each having a length (B) of 7 mm and a width (T) of 2 mm. Figure 3 shows the geometry of the test structure (top) and some inkjet-printed samples (bottom).

C. Materials

The printer used for printing the test structures is based on a custom-built piezo-driven four-axis positioning system NAMOSE. It has a working space of 400 mm x 150 mm x 40 mm, a repeatability of less than 1 μm and a maximum speed of 200 mm/s [5]. The NAMOSE system is controlled by a Beckhoff-CX2040 with TwinCAT, programmable logic controller (PLC) and numerical control (NC) axis controlling. For inkjet-printing, the positioning system is equipped with a piezo-electrically driven single nozzle Microfab print head (MJ-AL-01-50-8MX) with an orifice diameter of 50 μm [5]. A NC-task synchronizes the droplet frequency (f_d) with the axis velocity (v), while the droplet distance (d_d) is maintained at its set point. Furthermore, the NAMOSE system is equipped with a
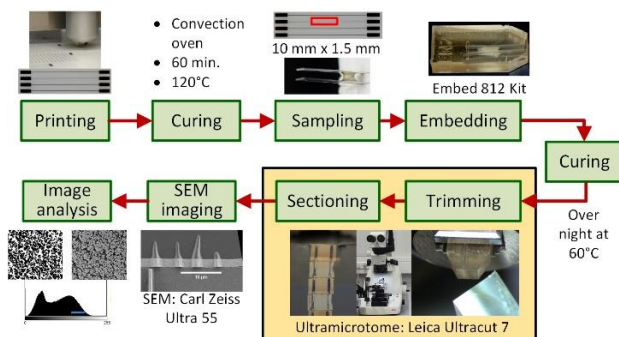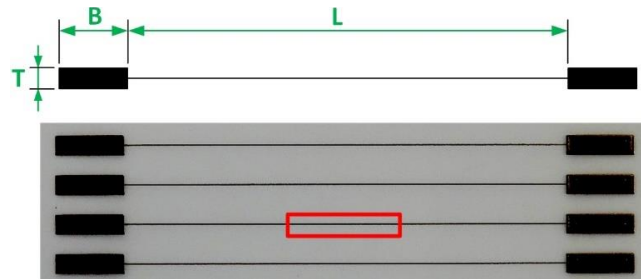
Figure 3. Inkjet test structure. Geometry (top), image of printed test structures (bottom), specimen geometry for sectioning (red box)

heated vacuum chuck and an optical observation system for controlling and adjusting droplet formation.

The silver-nanoparticle ink DGP 40LT-15C (Advanced Nano Products (ANP)) was purchased from Sigma Aldrich (736465 ALDRICH). The ink has a solid content of 30 - 35 wt % of silver nanoparticles of less than or equal to 50 nm diameter, a surface tension of 35 - 38 mN/m, a viscosity of about 10 - 17 mPa·s and is designed for application on polymer films. The manufacturer recommends a curing regime with 30 - 60 minutes at 120 - 150 °C. The main solvent of the ink is triethylene glycol monoethyl ether (TGME) [33]. The ink contains polyvinylpyrrolidone (PVP) as capping agent that leads to an electrostatic stabilization of the nanoparticles [14].

In the present work, two different PET-films were used as substrates. The 125 μm thick Melinex® ST506™ from DuPont Teijin Films is optimized for printed electronics. Both sides of this film are pre-treated for improved adhesion of inks [19]. The NB-TP-3GU100 from Mitsubishi Paper Mills is a 135 μm thick PET-film that is optimized for inkjet-printing of conductive structures based on silver nanoparticle dispersions. Due to its optimized nanoporous single side coating, it provides fast drying of water-based inks [34]. The thickness, morphology and the surface chemistry of this coating are not further specified by the supplier.

D. Printing samples

Test structures were printed on both substrates using the ink DGP 40LT-15C. The piezo-inkjet-device was actuated with a standard trapezoidal waveform. Figure 4 left illustrates the applied waveform. Figure 4 right shows the resulting droplet formation. For all samples, the waveform parameter t_{rise} was 3.0 μs, t_{dwell} was 28.0 μs and t_{fall} 3.0 μs.
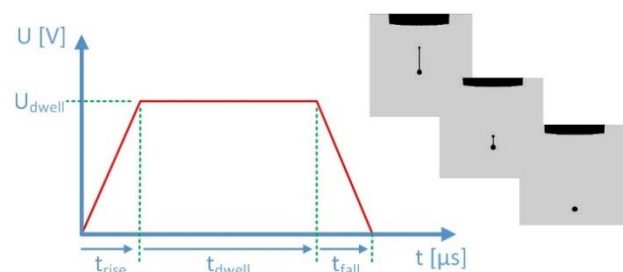
Figure 2. Workflow for the analysis of printed structures

Figure 4. Waveform parameters and droplet formation

TABLE I. PRINTING PARAMETERS

sample	substrate	d_d [µm]	T_S [°C]	v [mm/s]
A	Melinex® ST506™	147	80	50
B	Melinex® ST506™	13	80	50
C	NB-TP-3GU100	31	RT	10
D	NB-TP-3GU100	1	RT	10

For the samples A, C and D, U_{dwell} was 38.0 V. For sample B, U_{dwell} was 35.0 V.

Table I shows the printing parameters for four different samples. After printing, the samples were cured in a convection oven (Memmert UP 500) for about 60 min. at 120 °C.

After curing, the width of the central part of the test structure (see the red box in Figure 3) was measured by optical microscopy and image processing with the DIPLOM software that was developed at the KIT Institute for Applied Computer Science (IAI). The image processing yields the line width and its standard deviation which can be used as an indicator of the line edge quality.

E. Sample preparation for SEM-analysis

For analyzing the cross section in the central area of the printed traces, about 10 mm long and 1.5 mm wide rectangular specimen were cut from the printed test structures (see the red box in Figure 3).

As it is not possible at ambient conditions, to directly cut the flexible polymer with an ultramicrotome without delamination of the ink, the printed samples need to be embedded into a polymer in order to achieve proper sections. Two different specimens were embedded parallel to each other into one embedding mould.

As embedding resin, the Embed 812 Kit from Electron Microscopy Sciences was used. The filled embedding moulds were cured over night at 60 °C in a convection oven.

After polymerization, the resulting blocks with the embedded samples were removed from the moulds and then prepared for ultramicrotome sectioning. For this purpose, the blocks were trimmed in a Leica Ultracut 7 ultramicrotome using a standard glass trimming knife. Then, sections of 100 nm and 200 nm thickness were cut with the same instrument but with a Diatome Ultra 35° knife at ambient conditions. The knife boat was filled with double-distilled water during the cutting process. To avoid electrostatic charging of the sample, a Diatome static line 2 ionizer was used. The cut sections are floating on the water surface of the knife boat, where they can be subsequently picked up and placed on a silicon wafer for imaging in the scanning electron microscope (SEM).

For SEM imaging, an Ultra 55 (Carl Zeiss Microscopy, Oberkochen, Germany) was used. Particle density in the SEM images of the cross sections was measured with the software package Fiji [35].

Figure 5 illustrates the approach to determine the particle density by image segmentation. The threshold for the segmentation was manually selected for different details of a SEM-image of a cross section. The particles density in the sectional plane was calculated for each detail.
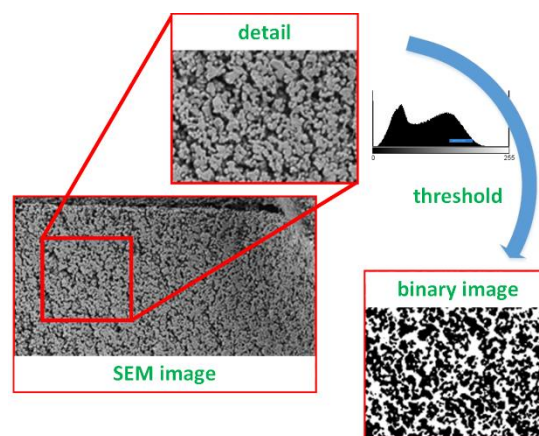

Figure 5. Determination scheme of the nanoparticle density

III. RESULTS AND DISCUSSION

A. Printing and curing

In a preliminary test, it was found that the behavior of the ink after deposition at room temperature is completely different on the two different substrates. Although the initial wetting seems to be good, printing on the Melinex® ST506™ substrate is followed by a continuous parasitic spreading combined with a resulting shape similar to a coffee-ring effect. This results in very flat, broad and fringed traces, with poor edge quality. The nanoporous coating of the PET-film from Mitsubishi Paper Mills avoids this ink spreading over a broad range of droplet-distances d_d. A considerable trace height can be achieved, even for narrow traces. Optimizing the droplet-distance (d_d), it is even possible to print continuous traces with a width of less than the diameter of a single droplet. Figure 6 shows microscope images of this preliminary test. The printing parameters were the same for both substrates: the jetting frequency (f_d) was 2000 Hz, the axis speed (v) was 100 mm/s and the droplet-distance (d_d) results in 50 µm. The silver trace on Melinex® ST506™ (see Figure 6 left) shows a poor edge quality, a width of about 1180 µm and a height in the range of about 100 nm, whereas the trace printed on NB-TP-3GU100 (see Figure 6 right) has a good edge quality at a width of about 88 µm and a height of about 1140 nm.
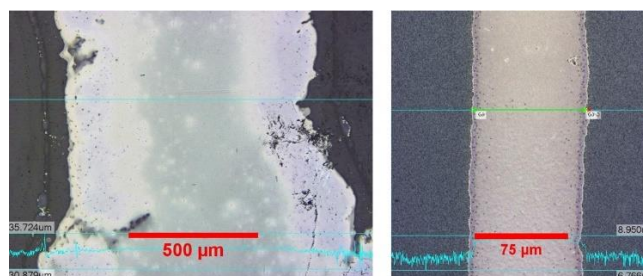

Figure 6. Microscope images of printed silver ink traces at room temperature on Melinex® ST506™ (left) and on NB-TP-3GU100 (right)

In further tests, it was found that printing on Melinex® ST506™, with 80 °C substrate temperature results in much better trace quality. This parameter was maintained for all subsequent tests with this substrate.

Concerning the sintering in a convection oven, an irreversible warping of the NB-TP-3GU100 can be observed when heating above T_g of PET. This warpage potentially induces an initial strain into the printed structures, which may lead to damages such as cracks and delamination. A possible explanation for this effect could be different thermal expansion coefficients of the single-side nanoporous coating and the PET bulk material. The Melinex® ST506™ substrate does not show such an effect.

B. Ultramicrotome sectioning

Figure 7 shows the block with the embedded specimens (left, a and b), the top of the block during trimming with the glass knife (center, c) and a section directly after cutting (right).

200 nm sections can be cut reproducibly but with a significant wrinkling of the embedding material along the edges of the embedded specimens (see Figure 7 right, d and e). Lower section thicknesses led to delamination between specimen and embedding resin due to this wrinkling.

Different cutting directions were evaluated with respect to the sample orientation in the block: perpendicular, parallel and at an angle to the embedded substrate plane. Figure 8 shows typical results indicating the effect of the cutting direction (red arrows).

When cutting is performed perpendicular to the substrate plane, the interface between the ink and the substrate is being compressed and can therefore not be used for further investigation of the interface. Additionally, this section shows many wrinkles and dominant knife marks (see Figure 8 left). In contrast, sections obtained when cutting parallel to the substrate plane, show less wrinkles and knife marks (see Figure 8 center). It is assumed that this cutting direction introduces fewer mechanical stresses to the interface between ink and substrate. The sections obtained, when cutting at an angle of about 26° to the substrate plane, were also acceptable (see Figure 8 right). The embedded NB-TP-3GU100 substrate (see Figure 8 a and c) produces much more wrinkles than the Melinex® ST506™ (see Figure 8 b and d). We suppose that Melinex® film is harder than the Mitsubishi film due to its heat and surface
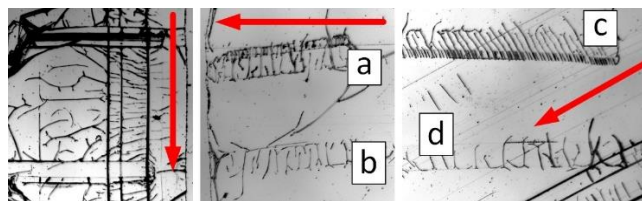
Figure 8. Influence of the cutting direction on the section morphology and the specimens (a and c: NB-TP-3GU100; b and d: Melinex® ST506™). Perpendicular (left), parallel (center) and 26° (right) to substrate plane (arrows indicate cutting direction)

treatment. This can explain why the sections of NB-TP-3GU100 specimen show a stronger wrinkling than the Melinex® substrate.

C. SEM analysis and image segmentation

Despite varying the cutting direction, a certain degree of section wrinkling was unavoidable. This led to a degradation of the sections in terms of cracks. Sometimes delamination occurred in the section while cutting. Figure 9 shows a section from a NB-TP-3GU100 substrate cut parallel to the substrate plane (I). It can be seen that the substrate was torn during the cutting process (see Figure 9 I) and the printed ink delaminates from the coated substrate at the locations of the wrinkles (II and III).

Nevertheless, there are enough regions suitable for further analysis (compare Figure 9 II and III), since the cutting preserved the nanostructure of the cross section.

Table II summarizes some of the results obtained from the analysis of images from SEM and optical microscopy of the printed samples.

Using the SEM-images, the line width was measured in the cross sections. It can be seen that there is a discrepancy between both results for the line width. For the samples B and D, the discrepancy is stronger than for the other samples. The samples B and D were taken from the line ends, where a decrease in line width can be detected for both samples via optical microscopy. Therefore, the line widths measured using the SEM-images cannot be compared to the line width obtained from the optical scanning of the printed and
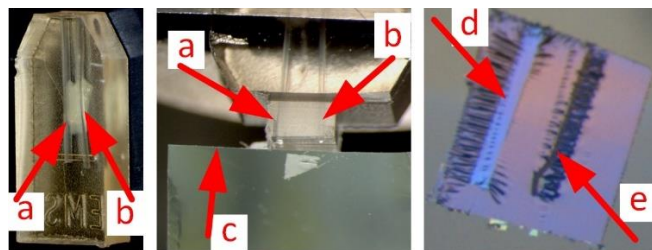

Figure 7. Sample preparation by ultramicrotome sectioning. Embedded specimens (a and b), trimming (center) with a glass knife (c) and 200 nm thin section floating on the water in the knife boat (right); Wrinkling of the embedding material along the edges of the embedded specimens (d and e)
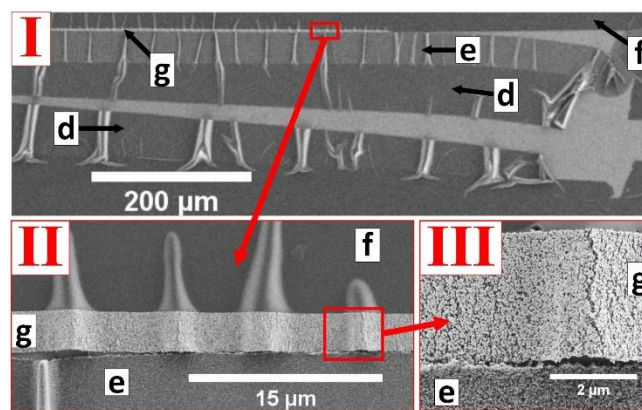

Figure 9. SEM images of a section containing a silver trace (g) printed on NB-TP-3GU100 substrate (d: bulk substrate, e: nanoporous coating, f: embedding resin); low magnification (I), high magnification (II, III); bulk substrate delamination (I); cracks and delamination of conductive traces (II, III)

TABLE II. RESULTS

Sample	Line width (REM, section) [μm]	Line width (opt., middle) [μm]	Ink layer thickness (REM) [nm]	Cutting angle [°]
A	155,2	205,1 +/- 4,4	182,2 +/- 18	5,9
B	273,2	607,74 +/- 93	1705,0 +/-24	25,6
C	84,5	98,0 +/- 2,8	840,0 +/- 85	5,6
D	393,6	612,6 +/- 8	3719 +/- 20	28,9

sintered lines (as described in Section II.D).

In the case of the samples A and C that were taken from the middle of the lines, both values for the line width can be compared. For A, the line width measured from the REM-image is about 76 % of the line width calculated from the optical scanning data. For the sample C, this value is about 86 %. For both substrates, there is a wrinkling induced "shrinkage" of the measured line width in the range of 14 to 24 % of the line width due to the ultramicrotome-cutting process at an angle of about 6° between the cutting direction and the substrate's surface. The wrinkles coming out of the section plane are the results of that process. Table II also shows the results of the measurements of the ink layer thickness by SEM-image-analysis.

The ratio of the ink layer thickness and the line width is about 0.09 % for the narrow line printed on Melinex® ST506™ (sample A). This ratio is about 0.86 % for a narrow line printed on NB-TP-3GU100 (sample C). The wide line on Melinex® ST506™ achieves a ratio of ink layer thickness and line width of about 0.28 % (sample B) whereas this ratio is about 0.61 % for NB-TP-3GU100 (sample D). The actual cutting angles for all four samples are also given in Table II.

Figure 10 shows the cross section of the samples B (I) and D (II). The full low magnification cross section for each sample can be seen on the top, a detail image can be found on the bottom for each sample. Using such high magnification images from SEM the particle density of each
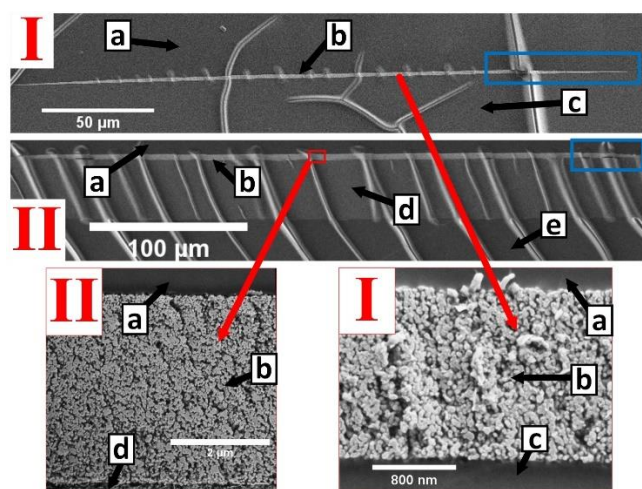

Figure 10. SEM images of sections containing the samples B (I; a: embedding resin, b: silver ink, c: substrate) and D (II; a: resin, b: silver ink, d: nanoporous coating, e: bulk substrate); low magnification (top) and high magnification images (bottom)
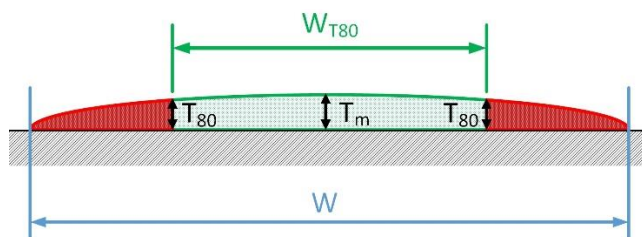

Figure 11. Off leveling of the cross section of a printed line towards its edges. T_m: ink layer thickness measured in the middle of the cross section; T_{80}: 80 % of the ink layer thickness T_m; W: line width; W_{T80}: width of the cross section segment for which the ink layer thickness is greater or equal to T_m

sample according to the procedure described above has been determined. The particle density of the conductive traces calculated for all four samples was between 58 % and 65 %. The particle density is slightly higher for structures printed on Melinex® ST506™ than on Mitsubishi NB-TP-3GU100. For the samples A and B the particle density is about 65 % and 61 %, respectively. In the case of the samples C and D, the particle density was calculated to about 60 % and 58 %.

Moreover, from these SEM images, it can be derived that the cross section of the traces printed on Melinex® ST506™ tapers off towards the line edges (see the blue box in Figure 10 I). In contrast, the height of the silver trace on NB-TP-3GU100 only decreases close to the edges (see the blue box in Figure 10 II). An off leveling ratio of the line's thickness towards its edges was determined for the different samples. Figure 11 illustrates the determination of the off leveling ratio. The ink layer thickness was measured in small steps starting in the middle of the cross section moving towards the edges. The two points T_{80} where the ink layer thickness falls below 80 % of the ink layer thickness in the middle of the cross section T_m delimit the segment W_{T80} of the cross section. Formula (1) defines the off leveling ratio OL.

$$OL = \frac{W - W_{T80}}{W} \cdot 100\ \% \qquad (1)$$

The obtained value gives an impression of the ink layer thickness across the line width. It can be seen, that the off leveling is stronger for the substrate Melinex® ST506™ than for the NB-TP-3GU100. For the sample B, the off leveling ratio is about 43.8 %, for the sample C, it is 24.4 % and for the sample D, the off leveling ratio is 24.6 %. The off leveling ratio seems to be characteristic for a given substrate (compare values for samples B and D) and independent of the line width (compare values for samples C and D).

Figure 12 shows SEM images of the samples A (I) and C (II). In the segment at the bottom of Figure 12 it can be seen that the ink layer thickness of the sample C (II) is higher than for sample A.

Figure 13 shows SEM images of one section containing both samples B and D. It can be seen that the wrinkling is stronger for the NB-TP-3GU100 substrate than for the Melinex® ST506™. In can be supposed that Melinex® ST506™ is stiffer than NB-TP-3GU100 and that the embedding resin is more or less as hard as Melinex®
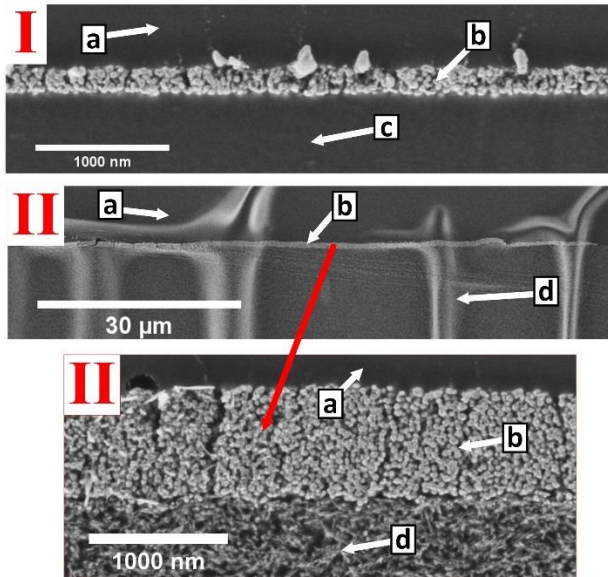
Figure 12. SEM images of sections containing the samples A (I; a: embedding resin, b: silver ink, c: substrate) and C (II; a: resin, b: silver ink, d: nanoporous coating); low magnification (top and bottom), high magnification (middle)

ST506™. This finding confirms the observation described above (Section III.B).

Moreover, Figure 13 I shows that in sample A larger silver particles have been ripped out of the conductive trace and are smeared into the embedding resin. This indicates that the embedding and cutting process have to be further optimized. Using different SEM- and optical microscope images, the the substrate thickness has been measured. For Melinex® ST506™ a substrate thickness of 127.9 µm +/- 2.0 µm was determined. The Mitsubishi NB-TP-3GU100 has a thickness of 138.2 +/- 2.5 µm, whereof the nanoporous layer is 38.3 µm +/- 1.0 µm.

The comparatively high thickness of this layer supports the hypothesis stated above (Section III.A) that this might be the main reason for the warping of the substrate after thermal sintering. There was no indication for sectioning or embedding process related changes of substrate thickness,
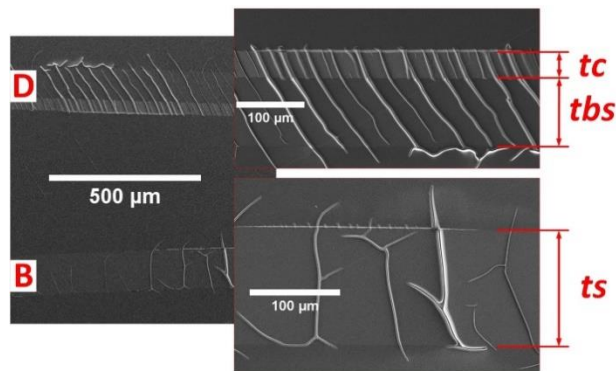

Figure 13. SEM image of the section containing the samples B and D (left, low magnification), segments of both samples (right top and bottom, tc: thickness of the coating, tbs: thickness of the bulk substrate, ts: thickness of the entire substrate; higher magnification)

neither for the bulk substrate nor for the porous coating. With proper cutting parameters (angle between cutting direction and substrate plane) the influence on the ink layer thickness should be minimal. Section wrinkling due to stiffness incompatibilities between substrate and embedding materials is probably the only remarkable deformation of the samples during the whole sectioning process.

IV. CONCLUSION AND OUTLOOK

A method was outlined for analyzing the nano- and microstructure of inkjet printed conductive traces on different polymer substrates using ultramicrotome sectioning and SEM imaging. Our results confirm the finding by Melo [4]. The sections produced showed wrinkling along the substrate plane partially leading to delamination. This may result from stiffness differences between the substrate material and the embedding resin, a parameter to be optimized in further investigations. Despite the resulting delaminations, there were enough regions that could be used for investigation of the nanoparticle network of the printed conductive traces. This indicates that with properly optimized embedding and cutting parameters, the described scheme is a promising method for analyzing thermal, mechanical and chemical influences on the morphology of printed metal nanoparticle inks and on the interface between substrate and ink.

REFERENCES

[1] M. Ungerer, W. Spomer, L. Veith, A. Fries, C. Debatin, I. Wacker et al., "Analysis of the cross section of inkjet-printed conductive tracks on PET films," ACHI 2017: The Tenth International Conference on Advances in Computer-Human Interactions, Nice, France. March 19 - 23, 2017, pp. 162–168.

[2] J. Perelaer and U. S. Schubert, "Novel approaches for low temperature sintering of inkjet-printed inorganic nanoparticles for roll-to-roll (R2R) applications," Journal of Materials Research, Vol. 28, No. 4, 2013, pp. 564–573. doi:10.1557/jmr.2012.419.

[3] J. Gierak, "Focused Ion Beam nano-patterning from traditional applications to single ion implantation perspectives," Nanofabrication, Vol. 1, No. 1, 2014. doi:10.2478/nanofab-2014-0004.

[4] L. G. de A. Melo, A. P. Hitchcock, V. Berejnov, D. Susac, J. Stumper and G. A. Botton, "Evaluating focused ion beam and ultramicrotome sample preparation for analytical microscopies of the cathode layer of a polymer electrolyte membrane fuel cell," Journal of Power Sources, Vol. 312, 2016, pp. 23–35. doi:10.1016/j.jpowsour.2016.02.019.

[5] M. Ungerer, U. Gengenbach, A. Hofmann and G. Bretthauer, "Comparative and systemic analysis of digital single nozzle printing processes for the manufacturing of functional microstructures," Proc. MikroSystemTechnik Kongress (MST 2015): MEMS, Mikroelektronik, Systeme, Karlsruhe. 10/26/2015 - 10/28/2015.

[6] J. Lessing, A. C. Glavan, S. B. Walker, C. Keplinger, J. A. Lewis and G. M. Whitesides, "Inkjet Printing of Conductive

Inks with High Lateral Resolution on Omniphobic "RF Paper" for Paper-Based Electronics and MEMS," Advanced Materials, Vol. 26, No. 27, 2014, pp. 4677–4682. doi:10.1002/adma.201401053.

[7] H.-H. Lee, K.-S. Chou and K.-C. Huang, "Inkjet printing of nanosized silver colloids," Nanotechnology, Vol. 16, No. 10, 2005, p. 2436. doi:10.1088/0957-4484/16/10/074.

[8] Y. Kawahara, S. Hodges, N.-W. Gong, S. Olberding and J. Steimle, "Building Functional Prototypes Using Conductive Inkjet Printing," IEEE Pervasive Comput., Vol. 13, No. 3, 2014, pp. 30–38. doi:10.1109/MPRV.2014.41.

[9] T. Öhlund, A. Schuppert, B. Andres, H. Andersson, S. Forsberg, W. Schmidt et al., "Assisted sintering of silver nanoparticle inkjet ink on paper with active coatings," RSC Advances, Vol. 5, No. 80, 2015, pp. 64841–64849. doi:10.1039/C5RA06626C.

[10] S. H. Ko, H. Pan, C. P. Grigoropoulos, C. K. Luscombe, J. M. J. Fréchet and D. Poulikakos, "All-inkjet-printed flexible electronics fabrication on a polymer substrate by low-temperature high-resolution selective laser sintering of metal nanoparticles," Nanotechnology, Vol. 18, No. 34, 2007, p. 345202. doi:10.1088/0957-4484/18/34/345202.

[11] M. Mikolajek, A. Friederich, C. Kohler, M. Rosen, A. Rathjen, K. Krüger et al., "Direct Inkjet Printing of Dielectric Ceramic/Polymer Composite Thick Films," Advanced Engineering Materials, Vol. 17, No. 9, 2015, pp. 1294–1301. doi:10.1002/adem.201400451.

[12] T. T. Baby, M. Rommel, F. von Seggern, P. Friederich, C. Reitz, S. Dehm et al., "Sub-50 nm Channel Vertical Field-Effect Transistors using Conventional Ink-Jet Printing," Advanced Materials, Vol. 29, No. 4, 2017. doi:10.1002/adma.201603858.

[13] J. Perelaer, R. Jani, M. Grouchko, A. Kamyshny, S. Magdassi and U. S. Schubert, "Plasma and Microwave Flash Sintering of a Tailored Silver Nanoparticle Ink, Yielding 60% Bulk Conductivity on Cost-Effective Polymer Foils," Advanced Materials, Vol. 24, No. 29, 2012, pp. 3993–3998. doi:10.1002/adma.201200899.

[14] H. Andersson, A. Manuilskiy, T. Unander, C. Lidenmark, S. Forsberg and H.-E. Nilsson, "Inkjet Printed Silver Nanoparticle Humidity Sensor With Memory Effect on Paper," IEEE Sensors J., Vol. 12, No. 6, 2012, pp. 1901–1905. doi:10.1109/JSEN.2011.2182044.

[15] J. Niittynen, R. Abbel, M. Mäntysalo, J. Perelaer, U. S. Schubert and D. Lupo, "Alternative sintering methods compared to conventional thermal sintering for inkjet printed silver nanoparticle ink," Thin Solid Films, Vol. 556, 2014, pp. 452–459. doi:10.1016/j.tsf.2014.02.001.

[16] G. L. Allen, R. A. Bayles, W. W. Gile and W. A. Jesser, "Small particle melting of pure metals," Thin Solid Films, Vol. 144, No. 2, 1986, pp. 297–308. doi:10.1016/0040-6090(86)90422-0.

[17] P. Buffat and J.-P. Borel, "Size effect on the melting temperature of gold particles," Phys. Rev. A, Vol. 13, No. 6, 1976, p. 2287. doi:10.1103/PhysRevA.13.2287.

[18] W. A. MacDonald, "Engineered films for display technologies," J. Mater. Chem., Vol. 14, No. 1, 2004, p. 4. doi:10.1039/b310846p.

[19] DuPont Teijin Films, "Product Information Melinex® ST506™," 2012. http://www.koenig-kunststoffe.de/produkte/melinex/melinex-r-st506.pdf, accessed 23 December 2017.

[20] W. A. MacDonald, M. K. Looney, D. MacKerron, R. Eveson, R. Adam, K. Hashimoto et al., "Latest advances in substrates for flexible electronics," Journal of the Society for Information Display, Vol. 15, No. 12, 2007, pp. 1075–1083. doi:10.1889/1.2825093.

[21] S. Magdassi, "Ink Requirements and Formulations Guidelines," In: S. Magdassi, Ed., The chemistry of inkjet inks, World Scientific Pub. Co, Singapore, Hackensack, N.J, 2010, pp. 19–41.

[22] D.-H. Lee, K.-T. Lim, E.-K. Park, J.-M. Kim and Y.-S. Kim, "Optimized ink-jet printing condition for stable and reproducible performance of organic thin film transistor," Microelectronic Engineering, Vol. 111, 2013, pp. 242–246. doi:10.1016/j.mee.2013.03.177.

[23] G. Li, R. C. Roberts and N. C. Tien, "Interlacing method for micro-patterning silver via inkjet printing," Proc. IEEE 13th Sensors Conference, Valencia, Spain. 2/11/2014 - 5/11/2014, pp. 1687–1690.

[24] F. Molina-Lopez, D. Briand and N. F. de Rooij, "All additive inkjet printed humidity sensors on plastic substrate," Sensors and Actuators B: Chemical, 166–167, 2012, pp. 212–222. doi:10.1016/j.snb.2012.02.042.

[25] D. Soltman and V. Subramanian, "Inkjet-printed line morphologies and temperature control of the coffee ring effect," Langmuir the ACS journal of surfaces and colloids, Vol. 24, No. 5, 2008, pp. 2224–2231. doi:10.1021/la7026847.

[26] I. Reinhold, C. E. Hendriks, R. Eckardt, J. M. Kranenburg, J. Perelaer, R. R. Baumann et al., "Argon plasma sintering of inkjet printed silver tracks on polymer substrates," Journal of Materials Chemistry, Vol. 19, No. 21, 2009, pp. 3384–3388. doi:10.1039/B823329B.

[27] J. Perelaer, M. Klokkenburg, C. E. Hendriks and U. S. Schubert, "Microwave Flash Sintering of Inkjet-Printed Silver Tracks on Polymer Substrates," Advanced Materials, Vol. 21, No. 47, 2009, pp. 4830–4834. doi:10.1002/adma.200901081.

[28] S. Magdassi, M. Grouchko, O. Berezin and A. Kamyshny, "Triggering the sintering of silver nanoparticles at room temperature," ACS nano, Vol. 4, No. 4, 2010, pp. 1943–1948. doi:10.1021/nn901868t.

[29] B.-J. Kim, T. Haas, A. Friederich, J.-H. Lee, D.-H. Nam, J. R. Binder et al., "Improving mechanical fatigue resistance by optimizing the nanoporous structure of inkjet-printed Ag electrodes for flexible devices," Nanotechnology, Vol. 25, No. 12, 2014, p. 125706. doi:10.1088/0957-4484/25/12/125706.

[30] N. Marjanović, "Hybrid electronics systems by CSEM," Proc. 8th International Exhibition and Conference for the Printed Electronics Industry (LOPEC 2016): Technical Conference, München, 2016.

[31] U. Gengenbach, Markus Dickerhof, Liane Koker, Jörg Nagel, Ingo Sieber, Georg Schwartz et al., "A toolbox for multifunctional multilayer printed systems," Proc. MikroSystemTechnik Kongress (MST 2015): MEMS, Mikroelektronik, Systeme, Karlsruhe. 10/26/2015 - 10/28/2015.

[32] S. Merilampi, T. Laine-Ma and P. Ruuskanen, "The characterization of electrically conductive silver ink patterns on flexible substrates," Microelectronics Reliability, Vol. 49, No. 7, 2009, pp. 782–790. doi:10.1016/j.microrel.2009.04.004.

[33] Advanced Nano Products (ANP), "Nano-Silver Ink for Inkjet Printing," 2017. http://anapro.com/eng/product/silver_inkjet_ink.html, accessed 27 February 2017.

[34] Mitsubishi Paper Mills, "Technical Data Sheet: Mitsubishi Nano Benefit Series NB-TP-3GU100," 2014. https://www.mitsubishi-paper.com/fileadmin/user_upload/PrePress/downloads/silver_nano/PET_Film_NB-TP-3GU100.pdf, accessed 23 December 2017.

[35] J. Schindelin, I. Arganda-Carreras, E. Frise, V. Kaynig, M. Longair, T. Pietzsch et al., "Fiji: an open-source platform for biological-image analysis," Nature Methods, Vol. 9, No. 7, 2012, pp. 676–682. doi:10.1038/nmeth.2019.